Research Article

Nano Research
2021, 14(12): 4828–4832

ISSN 1998-0124 CN 11-5974/O4
https://doi.org/10.1007/s12274-021-3436-6

Ni-based catalysts derived from layered-double-hydroxide nanosheets for efficient photothermal CO_2 reduction under flow-type system

Zhenhua Li[1,2], Run Shi[2,3], Jiaqi Zhao[2,4], and Tierui Zhang[1] (✉)

[1] College of Chemistry, Central China Normal University, Wuhan 430079, China
[2] Key Laboratory of Photochemical Conversion and Optoelectronic Materials, Technical Institute of Physics and Chemistry, Chinese Academy of Sciences, Beijing 100190, China
[3] Key Laboratory of Thermal Management and Energy Utilization of Aircraft, Ministry of Industry and Information Technology, Nanjing 210016, China
[4] Center of Materials Science and Optoelectronics Engineering, University of Chinese Academy of Sciences, Beijing 100049, China

Received: 21 January 2021 / **Revised:** 23 February 2021 / **Accepted:** 3 March 2021

ABSTRACT

Photothermal CO_2 reduction is an efficient and sustainable catalytic path for CO_2 treatment. Here, we successfully fabricated a novel series of Ni-based catalysts (Ni-*x*) via H_2 reduction of NiAl-layered double hydroxide nanosheets at temperatures (*x*) ranging from 300 to 600 °C. With the increase of the reduction temperature, the methane generation rate of the Ni-*x* catalyst for photothermal CO_2 hydrogenation gradually increased under ultraviolet-visible-infrared (UV–vis–IR) irradiation in a flow-type system. The Ni-600 catalyst showed a CO_2 conversion of 78.4%, offering a CH_4 production rate of 278.8 mmol·g^{-1}·h^{-1}, with near 100% selectivity and 100 h long-term stability. Detailed characterization analyses showed metallic Ni nanoparticles supported on amorphous alumina are the catalytically active phase for CO_2 methanation. This study provides a possibility for large-scale conversion and utilization of CO_2 from a sustainable perspective.

KEYWORDS

photothermal CO_2 hydrogenation, Ni-based catalysts, layered double hydroxide, photocatalysis, solar-to-fuel

1 Introduction

Sunlight as a clean energy, has been widely recognized as one of the most promising alternatives to fossil-fuel-based energy sources [1–3]. Carbon dioxide (CO_2) is a profuse and cheap C1 raw material as well as a powerful greenhouse gas [4–6]. Converting it to fuels or commodity chemicals (such as methane (CH_4), methanol, ethanol, formic acid, etc.) provides a feasible and attractive strategy to meet global energy demands while mitigating anthropogenic climate change [7–9]. Among many target products, CH_4 is a widely used vehicle fuel, for heat and intermediate to obtain other chemicals [10, 11]. Converting CO_2 into CH_4 through methanation has great significance for mitigating CO_2 emissions [12, 13]. Photocatalytic CO_2 reduction is gaining increasing interest owing to its advantage of using sunlight as the primary energy source [14–16]. In early years, Honda et al. using semiconductor TiO_2 successfully converted CO_2 into organic compounds under ultraviolet irradiation [17]. From then on, a large number of efforts have been focused on this reaction [18–21]. However, photocatalytic CO_2 conversion is still a challenging task due to its intrinsic limitation of sluggish multiple e^-/h^+ transfer process, and poor ability of using wide solar spectrum [22, 23]. These photocatalysts usually suffered from low conversion rates and low production yields, which are usually at the micromoles level within 1 h of irradiation [24–27].

Compared to photocatalytic CO_2 reduction, photothermal technology has shown much higher production yields of C1 (like CO or CH_4) even under mild conditions [28–31]. Photothermal effect over metallic structures exhibits unprecedented ability to convert visible and even near-infrared (NIR) light into heat energy, which inspires us to find new ways to substantially improve the light-driven CO_2 conversion efficiency. Recently, Ozin and co-workers demonstrated that Ru nanoparticles sputtered onto black silicon nanowire supports showed excellent photothermal performance of CO_2 methanation [32]. Other noble metal catalysts such as Rh/Al_2O_3, $Ru/NaTaO_2$ and $Pd@Nb_2O_5$ have also been demonstrated to exhibit good activities for the conversion of CO_2 to methane [21, 33, 34]. However, these noble metal catalysts were not conducive to further practical applications due to their high cost. Therefore, there is an urgent need to develop cheap catalysts to achieve efficient photothermal CO_2 methanation. Interestingly, García and co-workers reported that the Ni/SiO_2·Al_2O_3 (contains a mixture of Ni and NiO nanoparticles) with photocatalytic CO_2 methanation performance in a batch reactor [35]. However, the production yield was too low to satisfy the practical application under the flow system. Layered-double-hydroxide (LDH), a class of easily accessible two-dimensional (2D) crystal structure with versatility in chemical composition and well-controlled morphology,

Address correspondence to tierui@mail.ipc.ac.cn

offers an abundant terrace for the development of novel catalysts (reducing by H_2 or heating at air atmospheres) with accurately custom structural, compositional and electronic properties [36–38]. In particular, a topotactic transformation of LDH to metal nanoparticles supported on a metal oxide substrate will occur upon calcination under reductive conditions [39, 40]. In principle, using H_2 to reduce Ni-containing LDH nanosheets at raising temperatures should generate nickel nanoparticles loaded alumina suitable for photothermal CO_2 reduction, inspiring a detailed research.

Here, we have successfully prepared a series of Ni-based photothermal catalysts by thermal reduction NiAl-LDH nanosheets in H_2 atmosphere at temperatures ranging from 300 and 600 °C (the catalysts denoted as Ni-*x*, where *x* represents the reduction temperature). For CO_2 hydrogenation under ultraviolet–visible–infrared (UV–vis–IR) irradiation, Ni-600 showed a CO_2 conversion of 78.4% with excellent CH_4 selectivity of 99.5% (278.8 mmol·g^{-1}·h^{-1}). To our knowledge, the CO_2 methanation performance is superior to most light-driven CO_2 methanation catalysts reported to date (Table S1 in the Electronic Supplementary Material (ESM)). Under flow conditions, Ni-600 showed a good stability in the reaction 100 h test period. Detailed catalyst characterization studies revealed that Ni-600 is composed of metallic Ni nanoparticles loaded on an alumina support, and the formation of discrete metal nanoparticles underpins the high CH_4 selectivity. In addition, this reaction occurs through a photothermal mechanism driven by the solar. Results also showcased the potential of solar-driven photothermal CO_2 reduction in a flow-type system.

2 Results and discussion

Alumina supported metal catalysts have received much attention in the research community and been used in the CO_2 hydrogenation reaction due to alumina's well mechanical character, outstanding stability and gentle metal-support interaction with commonly used transition metal catalysts [41]. Therefore, Al^{3+} was chosen as another metal in the synthesis of LDH precursor. As shown in Fig. S1 in the ESM, the as-prepared NiAl-LDH nanosheets have a Ni:Al atomic ratio of 2:1, which is consistent with the ratio of raw materials. The Ni-*x* catalysts were subsequently obtained by reducing the NiAl-LDH nanosheets in a H_2/Ar (10/90, v/v) atmosphere at temperatures ranging from 300–600 °C. The ratios of Ni to Al in all samples are basically unchanged after the reduction process compared with the LDH precursor (Fig. S2 in the ESM). The H_2 reduction-induced topological transformation of the NiAl-LDH nanosheets was evaluated by X-ray diffraction (XRD) shown in Fig. 1(a). Ni-300 shows the feature peaks of NiO. Ni appears when the reduction temperature increases to 400 °C, but the main phase remains to be NiO. The intensity of metallic Ni component increases when the reduction temperature reaches 500 °C. At 600 °C, almost all NiO is converted into metallic Ni. Temperature programmed reduction (TPR) reveals an intense signal between 500–600 °C, corresponding to the reduction of supported NiO to metallic Ni nanoparticles (Fig. S3 in the ESM).

UV–vis–IR absorption spectra were collected for the Ni-*x* catalysts to examine their UV–vis–IR absorption abilities, as this property was very important of photothermal catalysts for CO_2 hydrogenation. As shown in Fig. 1(b), Ni-300 showed a characteristic absorption around 700 nm due to d–d transitions of NiO [42, 43]. For Ni-*x* catalysts with $x > 400$, due to possessing a unique black appearance (Fig. S4 in the ESM), they absorbed strongly in the UV–vis–IR region. The CO_2 hydrogenation (CO_2/H_2/Ar = 15/60/25) performance of the Ni-*x* catalysts were evaluated under UV–vis–IR light irradiation

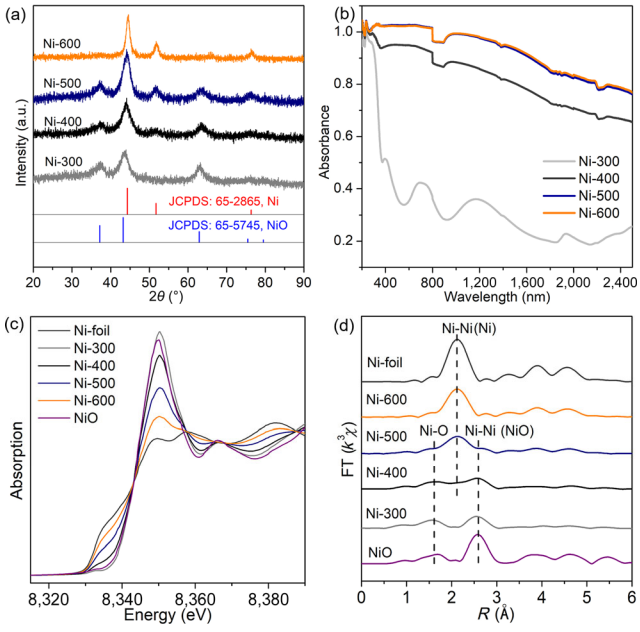

Figure 1 (a) XRD patterns, (b) UV–vis–IR spectra, (c) Ni K-edge XANES and (d) Ni K-edge EXAFS spectra for Ni-*x*.

in a flow-type reactor without external heating (Fig. S5 in the ESM). As presented in Fig. 2, Ni-300 shows a CO_2 conversion of 17.0%, with selectivities towards CH_4 and CO of about 80% and 20%, respectively. When the reduction temperature increases to 400 °C, the CO_2 conversion increases to 51% with excellent selectivity to CH_4 (~ 98.4%). Further increasing the reduction temperature from 400 to 600 results in a gradually improved CO_2 conversion from 51.9% to 78.8%, while keeping CH_4 as the main product (~ 99.3%). Ni-600 shows the best CH_4 production rate compared with other Ni-*x* catalysts (Fig. 2(d), and Fig. S6 in the ESM).

To clarify the possible contribution of photocatalytic and photothermal processes during CO_2 hydrogenation, we conducted a series of controlled experiments over Ni-600. Under UV–vis–IR irradiation, the temperature of the Ni-600 catalyst bed quickly rised to 290 °C (Figs. S7 and S8 in the ESM). At such a high temperature, it is almost certain that photothermally driven the

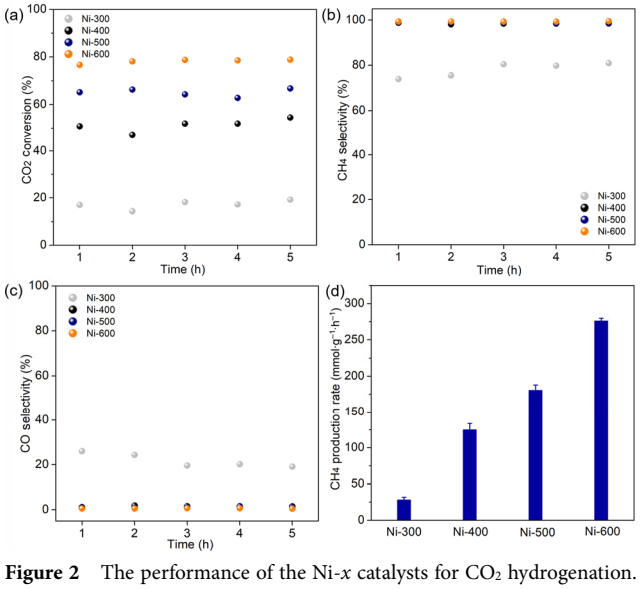

Figure 2 The performance of the Ni-*x* catalysts for CO_2 hydrogenation. (a) CO_2 conversion, (b) CH_4 selectivity, (c) CO selectivity, and (d) CH_4 yield rates. Reaction condition: H_2/CO_2/Ar = 60/15/25, flowrate 10 mL·min^{-1}, pressure 0.1 MPa, light intensity 2.63 W·cm^{-2}.

CO_2 hydrogenation reaction. A linear relationship is observed between the intensity of UV–vis–IR source and the catalyst surface temperature (Fig. S9 in the ESM). As shown in Figs. 3(a) and 3(b), at all temperatures studied, solar-driven the CO_2 hydrogenation achieved a very similar CO_2 conversion and products selectivity to the controlled thermocatalytic tests at same temperatures in dark. Above results conclusively demonstrate that the CO_2 methanation over Ni-600 mainly follows a photothermal pathway.

Ni K-edge X-ray absorption near-edge spectroscopy (XANES) and extended X-ray absorption fine structure (EXAFS) were used to study the structure evolution of the Ni-*x* (Figs. 1(c) and 1(d)). The metallic nickel and NiO powder were used as reference materials. The Ni K-edge XANES spectrum of Ni-300 is similar to the NiO reference, indicating that NiO was the dominant nickel species in this catalyst. The edge feature of metallic Ni appears at 400 °C, and gradually increases for catalysts reduced at higher temperatures. For Ni-600, the spectrum is very close to that of the Ni metal reference, indicating that metallic Ni is the dominant Ni-containing species in this catalyst. The conclusion was further confirmed by the EXAFS results (Fig. 1(d)). For Ni-300, the *R*-space plots is consistent with the NiO reference. When the reduction temperature increases from 400 to 600 °C, the intensity of Ni-Ni distance (metallic Ni) at 2.1Å gradually appears and increases, while the scattering of the Ni-O and Ni-Ni (NiO) distances at 1.6 and 2.6 Å gradually decreases. The Ni K-edge oscillation seen around 2–14 $Å^{-1}$ for the Ni-*x* (Fig. S10 in the ESM) further proves the transformation from Ni oxide to metallic Ni at high reduction temperatures.

Transmission electron microscopy (TEM) and high resolution TEM (HRTEM) were applied to probe the structure of Ni-600 (Fig. 4). The lattice fringes can be clearly seen in the HRTEM image (Fig. 4(b)), in which the 2.02 Å can be assigned to the (111) plane of Ni. Seen from the high-angle annular dark-field scanning TEM (HAADF-STEM) and energy dispersive X-ray spectroscopy (EDX) images in Figs. 4(c) and 4(d), the Ni nanoparticles with an average diameter of ~ 15 nm are uniformly dispersed on the Al_2O_3 support. The EDX line scan further demonstrates that the Ni nanoparticles consist of metallic Ni without oxidation (Fig. 4(e)).

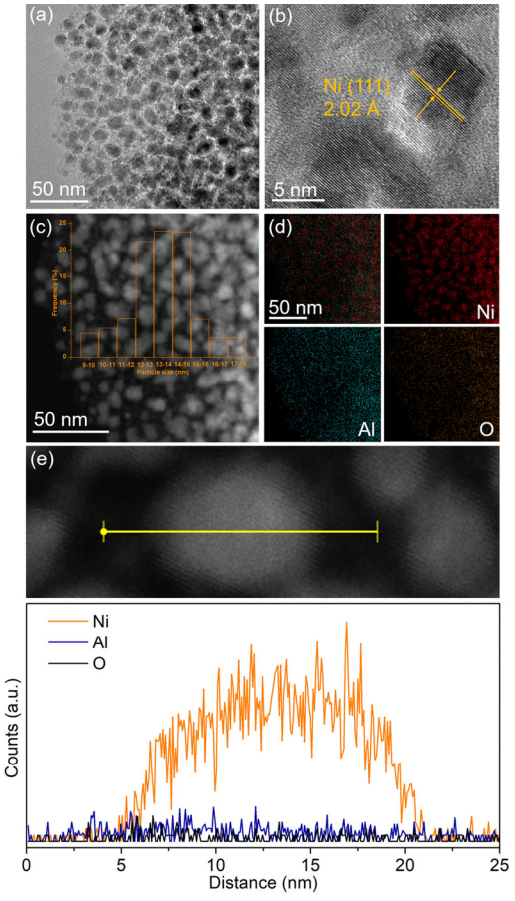

Figure 4 Characterization data for Ni-600. (a) and (b) HRTEM images, (c) HAADF-STEM image, inset in (c) is the particle size distribution of the metal Ni nanoparticles, (d) overlayed EDX element map and individual element maps for Ni, Al and O, (e) EDX line-scan element profile over one nanoparticle.

To further explore the photothermal catalytic stability of Ni-600. A 100 h long-term test was conducted in a flow reactor system, in which H_2 and CO_2 gases continuously flowed through the catalyst bed. As shown in Fig. 5, the CO_2 conversion rate

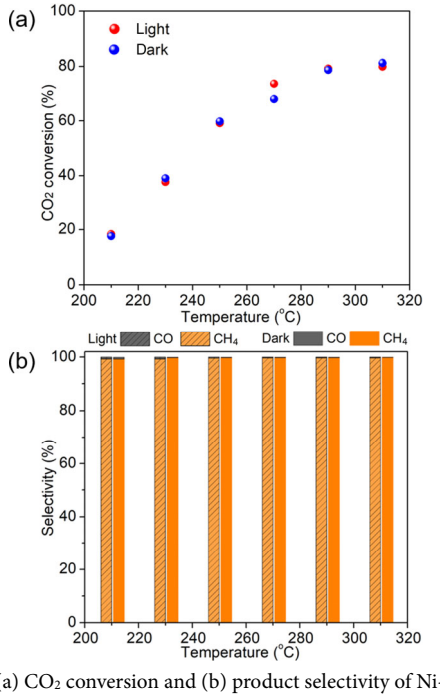

Figure 3 (a) CO_2 conversion and (b) product selectivity of Ni-600 under UV–vis–IR irradiation or direct heating at different reaction temperatures.

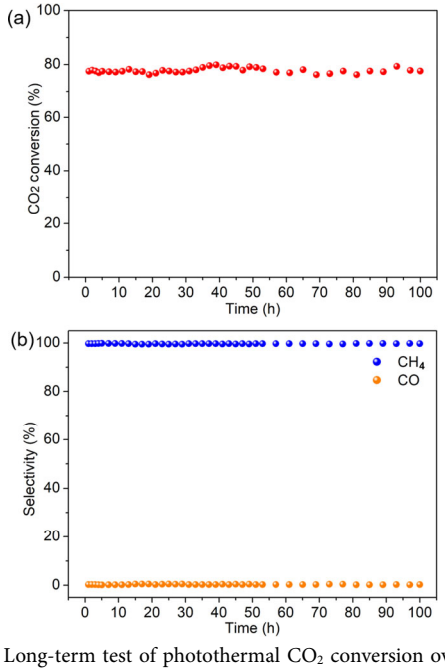

Figure 5 Long-term test of photothermal CO_2 conversion over Ni-600. (a) CO_2 conversion, (b) Product selectivity. Reaction condition: $H_2/CO_2/Ar$ = 60/15/25, flowrate 10 mL·min^{-1}, pressure 0.1 MPa, light intensity 2.63 W·cm^{-2}.

maintains at 78% with a CH_4 selectivity of 99.7% during 100 h operation. After the long-term stability test, the structure of Ni-600 showed negligible changes compared with the fresh Ni-600 (Figs. S11 and S12 in the ESM). This result confirms that the LDH-derived alumina supported metallic nickel catalyst is highly active and stable for photothermal CO_2 hydrogenation.

3 Conclusions

In conclusion, a series of Ni-based catalysts (Ni-*x*) have been successfully prepared by reducing NiAl-LDH nanosheets precursor at 300–600 °C. With the increase of reduction temperature, metallic Ni gradually becomes the dominant Ni species in the Ni-*x* catalysts. The Ni-600 catalyst showed the highest photothermal CO_2 conversion of 78.4% among all Ni-*x* catalysts, achieving a remarkable CH_4 selectivity of 99.5% at a CO_2 conversion specific activity of 278.8 $mmol \cdot g^{-1} \cdot h^{-1}$ under UV–vis–IR irradiation in a flow reaction system. This catalyst also exhibited an excellent catalytic stability, without obvious activity and structure changes during 100 h operation. This study develops LDH-derived low-cost catalysts to achieve photothermal CO_2 conversion with high activity, selectivity and stability, therefore opens a door for potential industrial applications of efficient and sustainable CO_2 photo-conversion.

Acknowledgements

The authors are grateful for financial support from the National Key Projects for Fundamental Research and Development of China (Nos. 2018YFB1502002, 2017YFA0206904, and 2017YFA0206900), the National Natural Science Foundation of China (Nos. 51825205, 51772305, 21871279, 21902168, and 52072382), the Beijing Natural Science Foundation (Nos. 2191002, and 2194089), the Strategic Priority Research Program of the Chinese Academy of Sciences (No. XDB17000000), the Royal Society-Newton Advanced Fellowship (No. NA170422), the International Partnership Program of Chinese Academy of Sciences (Nos. GJHZ1819 and GJHZ201974), the K. C. Wong Education Foundation, the Central China Normal University (No. 2020YBZZ019), the Youth Innovation Promotion Association of the CAS and the Open Fund of the Key Laboratory of Thermal Management and Energy Utilization of Aircraft, Ministry of Industry and Information Technology, Nanjing University of Aeronautics and Astronautics (No. CEPE2020014). The XAFS experiments were conducted in 1W1B beamline of Beijing Synchrotron Radiation Facility (BSRF).

Electronic Supplementary Material: Supplementary material (detailed synthetic procedures for NiAl-LDH and Ni-*x*, characterization, Figs. S1–S12) is available in the online version of this article at https://doi.org/10.1007/s12274-021-3436-6.

References

[1] Chueh, W. C.; Falter, C.; Abbott, M.; Scipio, D.; Furler, P.; Haile, S. M.; Steinfeld, A. High-flux solar-driven thermochemical dissociation of CO_2 and H_2O using nonstoichiometric ceria. *Science* **2010**, *330*, 1797–1801.

[2] Dasgupta, S.; Brunschwig, B. S.; Winkler, J. R.; Gray, H. B. Solar fuels editorial. *Chem. Soc. Rev.* **2013**, *42*, 2213–2214.

[3] Chen, G. B.; Waterhouse, G. I. N.; Shi, R.; Zhao, J. Q.; Li, Z. H.; Wu, L. Z.; Tung, C. H.; Zhang, T. R. From solar energy to fuels: recent advances in light-driven C_1 chemistry. *Angew. Chem., Int. Ed.* **2019**, *58*, 17528–17551.

[4] Jiang, X.; Nie, X. W.; Guo, X. W.; Song, C. S.; Chen, J. G. Recent advances in carbon dioxide hydrogenation to methanol via heterogeneous catalysis. *Chem. Rev.* **2020**, *120*, 7984–8034.

[5] He, M. Y.; Sun, Y. H.; Han, B. X. Green carbon science: Scientific basis for integrating carbon resource processing, utilization, and recycling. *Angew. Chem., Int. Ed.* **2013**, *52*, 9620–9633.

[6] Gattuso, J. P.; Magnan, A.; Billé, R.; Cheung, W. W. L.; Howes, E. L.; Joos, F.; Allemand, D.; Bopp, L.; Cooley, S. R.; Eakin, C. M. et al. Contrasting futures for ocean and society from different anthropogenic CO_2 emissions scenarios. *Science* **2015**, *349*, aac4722.

[7] Su, X.; Yang, X. F.; Huang, Y. Q.; Liu, B.; Zhang, T. Single-atom catalysis toward efficient CO_2 conversion to CO and formate products. *Acc. Chem. Res.* **2019**, *52*, 656–664.

[8] Zhao, T. X.; Hu, X. B.; Wu, Y. T.; Zhang, Z. B. Hydrogenation of CO_2 to formate with H_2: Transition metal free catalyst based on a Lewis pair. *Angew. Chem., Int. Ed.* **2019**, *58*, 722–726.

[9] Zhou, W.; Cheng, K.; Kang, J. C.; Zhou, C.; Subramanian, V.; Zhang, Q. H.; Wang, Y. New horizon in C1 chemistry: Breaking the selectivity limitation in transformation of syngas and hydrogenation of CO_2 into hydrocarbon chemicals and fuels. *Chem. Soc. Rev.* **2019**, *48*, 3193–3228.

[10] Miguel, C. V.; Mendes, A.; Madeira, L. M. Intrinsic kinetics of CO_2 methanation over an industrial nickel-based catalyst. *J. CO_2 Util.* **2018**, *25*, 128–136.

[11] Götz, M.; Lefebvre, J.; Mörs, F.; Koch, A. M.; Graf, F.; Bajohr, S.; Reimert, R.; Kolb, T. Renewable power-to-gas: A technological and economic review. *Renew. Energ.* **2016**, *85*, 1371–1390.

[12] Li, Y. G.; Hao, J. C.; Song, H.; Zhang, F. Y.; Bai, X. H.; Meng, X. G.; Zhang, H. Y.; Wang, S. F.; Hu, Y.; Ye, J. H. Selective light absorber-assisted single nickel atom catalysts for ambient sunlight-driven CO_2 methanation. *Nat. Commun.* **2019**, *10*, 2359.

[13] Chu, S.; Majumdar, A. Opportunities and challenges for a sustainable energy future. *Nature* **2012**, *488*, 294–303.

[14] Pan, Y. X.; You, Y.; Xin, S.; Li, Y. T.; Fu, G. T.; Cui, Z. M.; Men, Y. L.; Cao, F. F.; Yu, S. H.; Goodenough, J. B. Photocatalytic CO_2 reduction by carbon-coated indium-oxide nanobelts. *J. Am. Chem. Soc.* **2017**, *139*, 4123–4129.

[15] Zhao, Y. F.; Chen, G. B.; Bian, T.; Zhou, C.; Waterhouse, G. I. N.; Wu, L. Z.; Tung, C. H.; Smith, L. J.; O'Hare, D.; Zhang, T. R. Defect-rich ultrathin ZnAl-layered double hydroxide nanosheets for efficient photoreduction of CO_2 to CO with water. *Adv. Mater.* **2015**, *27*, 7824–7831.

[16] Hu, B. B.; Guo, Q.; Wang, K.; Wang, X. T. Enhanced photocatalytic activity of porous In_2O_3 for reduction of CO_2 with H_2O. *J. Mater. Sci.: Mater. Electron.* **2019**, *30*, 7950–7962.

[17] Inoue, T.; Fujishima, A.; Konishi, S.; Honda, K. Photoelectrocatalytic reduction of carbon dioxide in aqueous suspensions of semiconductor powders. *Nature* **1979**, *277*, 637–638.

[18] Wan, L. L.; Zhou, Q. X.; Wang, X.; Wood, T. E.; Wang, L.; Duchesne, P. N.; Guo, J. L.; Yan, X. L.; Xia, M. K.; Li, Y. F. et al. Cu_2O nanocubes with mixed oxidation-state facets for (photo)catalytic hydrogenation of carbon dioxide. *Nat. Catal.* **2019**, *2*, 889–898.

[19] Robatjazi, H.; Zhao, H. Q.; Swearer, D. F.; Hogan, N. J.; Zhou, L. N.; Alabastri, A.; McClain, M. J.; Nordlander, P.; Halas, N. J. Plasmon-induced selective carbon dioxide conversion on earth-abundant aluminum-cuprous oxide antenna-reactor nanoparticles. *Nat. Commun.* **2017**, *8*, 27.

[20] Kong, T. T.; Jiang, Y. W.; Xiong, Y. J. Photocatalytic CO_2 conversion: What can we learn from conventional CO_x hydrogenation? *Chem. Soc. Rev.* **2020**, *49*, 6579–6591.

[21] Li, M.; Li, P.; Chang, K.; Wang, T.; Liu, L. Q.; Kang, Q.; Ouyang, S. X.; Ye, J. H. Highly efficient and stable photocatalytic reduction of CO_2 to CH_4 over Ru loaded $NaTaO_3$. *Chem. Commun.* **2015**, *51*, 7645–7648.

[22] Tu, W. G.; Zhou, Y.; Zou, Z. G. Photocatalytic conversion of CO_2 into renewable hydrocarbon fuels: State-of-the-art accomplishment, challenges, and prospects. *Adv. Mater.* **2014**, *26*, 4607–4626.

[23] Indrakanti, V. P.; Kubicki, J. D.; Schobert, H. H. Photoinduced activation of CO_2 on Ti-based heterogeneous catalysts: Current state, chemical physics-based insights and outlook. *Energy Environ. Sci.* **2009**, *2*, 745–758.

[24] Ali, S.; Lee, J.; Kim, H.; Hwang, Y.; Razzaq, A.; Jung, J. W.; Cho, C. H.; In, S. I. Sustained, photocatalytic CO_2 reduction to CH_4 in

a continuous flow reactor by earth-abundant materials: Reduced titania-Cu_2O Z-scheme heterostructures. *Appl. Catal. B: Environ.* **2020**, *279*, 119344.

[25] Melsheimer, J.; Guo, W.; Ziegler, D.; Wesemann, M.; Schlögl, R. Methanation of carbon dioxide over Ru/titania at room temperature: Explorations for a photoassisted catalytic reaction. *Catal. Lett.* **1991**, *11*, 157–168.

[26] Wang, L.; Wan, J. W.; Zhao, Y. S.; Yang, N. L.; Wang, D. Hollow multi-shelled structures of Co_3O_4 dodecahedron with unique crystal orientation for enhanced photocatalytic CO_2 reduction. *J. Am. Chem. Soc.* **2019**, *141*, 2238–2241.

[27] Wu, L. Y.; Mu, Y. F.; Guo, X. X.; Zhang, W.; Zhang, Z. M.; Zhang, M.; Lu, T. B. Encapsulating perovskite quantum dots in iron-based metal-organic frameworks (MOFs) for efficient photocatalytic CO_2 reduction. *Angew. Chem., Int. Ed.* **2019**, *58*, 9491–9495.

[28] Song, C. Q.; Liu, X.; Xu, M.; Masi, D.; Wang, Y. G.; Deng, Y. C.; Zhang, M. T.; Qin, X. T.; Feng, K.; Yan, J. et al. Photothermal conversion of CO_2 with tunable selectivity using Fe-based catalysts: From oxide to carbide. *ACS Catal.* **2020**, *10*, 10364–10374.

[29] Wang, L.; Dong, Y. C.; Yan, T. J.; Hu, Z. X.; Jelle, A. A.; Meira, D. M.; Duchesne, P. N.; Loh, J. Y. Y.; Qiu, C. Y.; Storey, E. E. et al. Black indium oxide a photothermal CO_2 hydrogenation catalyst. *Nat. Commun.* **2020**, *11*. 2432.

[30] Xu, Y. F.; Duchesne, P. N.; Wang, L.; Tavasoli, A.; Jelle, A. A.; Xia, M. K.; Liao, J. F.; Kuang, D. B.; Ozin, G. A. High-performance light-driven heterogeneous CO_2 catalysis with near-unity selectivity on metal phosphides. *Nat. Commun.* **2020**, *11*, 5149.

[31] Qi, Y. H.; Song, L. Z.; Ouyang, S. X.; Liang, X. C.; Ning, S. B.; Zhang, Q. Q.; Ye, J. H. Photoinduced defect engineering: Enhanced photothermal catalytic performance of 2D black In_2O_{3-x} nanosheets with bifunctional oxygen vacancies. *Adv. Mater.* **2020**, *32*, 1903915.

[32] O'Brien, P. G.; Sandhel, A.; Wood, T. E.; Jelle, A. A.; Hoch, L. B.; Perovic, D. D.; Mims, C. A.; Ozin, G. A. Photomethanation of gaseous CO_2 over Ru/silicon nanowire catalysts with visible and near-infrared photons. *Adv. Sci.* **2014**, *1*, 1400001.

[33] Zhang, X.; Li, X. Q.; Zhang, D.; Su, N. Q.; Yang, W. T.; Everitt, H. O.; Liu, J. Product selectivity in plasmonic photocatalysis for carbon dioxide hydrogenation. *Nat. Commun.* **2017**, *8*, 14542.

[34] Jia, J.; Wang, H.; Lu, Z. L.; O'Brien, P. G.; Ghoussoub, M.; Duchesne, P.; Zheng, Z. Q.; Li, P. C.; Qiao, Q.; Wang, L. et al. Photothermal catalyst engineering: Hydrogenation of gaseous CO_2 with high activity and tailored selectivity. *Adv. Sci.* **2017**, *4*, 1700252.

[35] Sastre, F.; Puga, A. V.; Liu, L. C.; Corma, A.; Garcia, H. Complete photocatalytic reduction of CO_2 to methane by H_2 under solar light irradiation. *J. Am. Chem. Soc.* **2014**, *136*, 6798–6801.

[36] Adachi-Pagano, M.; Forano, C.; Besse, J. P. Synthesis of Al-rich hydrotalcite-like compounds by using the urea hydrolysis reaction-control of size and morphology. *J. Mater. Chem.* **2003**, *13*, 1988–1993.

[37] Fogg, A. M.; Rohl, A. L.; Parkinson, G. M.; O'Hare, D. Predicting guest orientations in layered double hydroxide intercalates. *Chem. Mater.* **1999**, *11*, 1194–1200.

[38] Gao, W.; Zhao, Y. F.; Chen, H. R.; Chen, H.; Li, Y. W.; He, S.; Zhang, Y. K.; Wei, M.; Evans, D. G.; Duan, X. Core-shell Cu@(CuCo-alloy)/Al_2O_3 catalysts for the synthesis of higher alcohols from syngas. *Green Chem.* **2015**, *17*, 1525–1534.

[39] Li, Z. H.; Liu, J. J.; Zhao, Y. F.; Shi, R.; Waterhouse, G. I. N.; Wang, Y. S.; Wu, L. Z.; Tung, C. H.; Zhang, T. R. Photothermal hydrocarbon synthesis using alumina-supported cobalt metal nanoparticle catalysts derived from layered-double-hydroxide nanosheets. *Nano Energy* **2019**, *60*, 467–475.

[40] Zhao, M. Q.; Zhang, Q.; Zhang, W.; Huang, J. Q.; Zhang, Y. H.; Su, D. S.; Wei, F. Embedded high density metal nanoparticles with extraordinary thermal stability derived from guest-host mediated layered double hydroxides. *J. Am. Chem. Soc.* **2010**, *132*, 14739–14741.

[41] Chen, G. B.; Gao, R.; Zhao, Y. F.; Li, Z. H.; Waterhouse, G. I. N.; Shi, R.; Zhao, J. Q.; Zhang, M. T.; Shang, L.; Sheng, G. Y. et al. Alumina-supported CoFe alloy catalysts derived from layered-double-hydroxide nanosheets for efficient photothermal CO_2 hydrogenation to hydrocarbons. *Adv. Mater.* **2018**, *30*, 1704663.

[42] Gorschlüter, A.; Merz, H. Locallied *d-d* excitations in NiO(100) and CoO(100). *Phys. Rev. B* **1994**, *49*, 17293–17302.

[43] Tan, L.; Xu, S. M.; Wang, Z. L.; Xu, Y. Q.; Wang, X.; Hao, X. J.; Bai, S.; Ning, C. J.; Wang, Y.; Zhang, W. K. et al. Highly selective photoreduction of CO_2 with suppressing H_2 evolution over monolayer layered double hydroxide under irradiation above 600 nm. *Angew. Chem., Int. Ed.* **2019**, *58*, 11860–11867.